energy&fuels

pubs.acs.org/EF Article

Perylenediimide-Incorporated Covalent Triazine Framework: A Highly Conductive Carbon Support for Copper Single-Atom Catalysts in Electrocatalytic CO_2 Conversion

Sebastian Raja,* Gelson T. S. T. da Silva, Eduardo A. Reis, Jean C. da Cruz, Anelisse Brunca Silva, Marcelo B. Andrade, Govindasami Periyasami, Perumal Karthikeyan, Igor F. Perepichka, Lucia Helena Mascaro, and Caue Ribeiro*

Cite This: https://doi.org/10.1021/acs.energyfuels.3c03268 Read Online

ACCESS | Metrics & More | Article Recommendations | Supporting Information

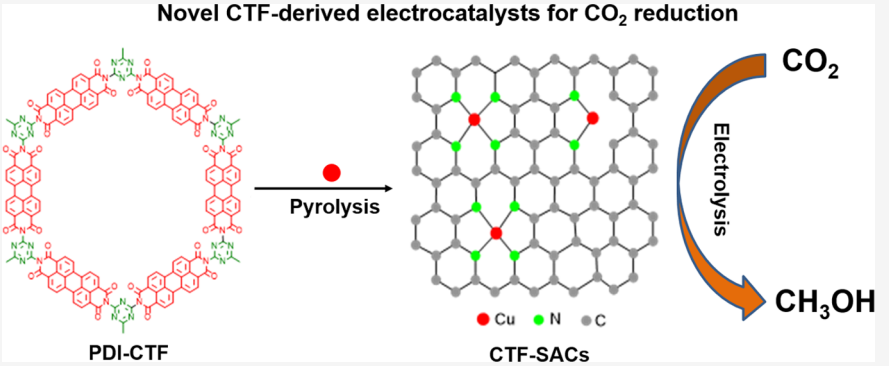

ABSTRACT: Here, we show that a perylenediimide-incorporated covalent triazine framework (PDI-CTF) leads to an adequate conductive carbon support for copper single-atom catalysts (Cu-SACs), allowing the selective electroreduction of CO_2 to methanol. CTF-Cu-SACs converted CO_2 into methanol with a faradaic efficiency of 72.6% at a low overpotential (0.2 V vs RHE). While increasing the overpotential (0.2 to −0.4 V vs RHE), CTF-Cu-SACs promoted syngas (CO and H_2) production with faradaic efficiencies of 53.2 and 39.5%, respectively. Moreover, CTF-Cu-SACs led to robust catalytic stability for 20 h of continuous electrolysis in an aqueous solution. Notably, it was observed that additional nitrogen doping to the PDI-CTF profoundly influences product selectivity, possibly due to the synergetic effect of highly conductive pyrolyzed CTF and N-chelating ligands with rich active sites. Our results indicate that the PDI-CTF-based Cu-SACs provide abundant active sites for CO_2 adsorption, thus enhancing intermolecular ion and charge transportation that efficiently reduces CO_2 into methanol in an aqueous system.

INTRODUCTION

Carbon dioxide (CO_2) accumulation in the atmosphere is a critical factor for global warming, becoming a major environmental threat.[1] Alleviating CO_2 emissions and tackling climate change risks are urgent need. Conversion of CO_2 into value-added products using renewable energy sources via modern approaches is a promising strategy to address this issue.[2−4] Electrocatalytic CO_2 reduction reactions (CO_2RRs) have gained remarkable attention in heterogeneous catalysis due to their cost-effectiveness, ecofriendliness, and energy-efficient features.[5−7] CO_2RR yields various hydrocarbons and fuels, including CO, CH_4, CH_3OH, CO, HCOOH (C_1 products), acetic acid, ethylene, ethanol, and propanol (C_2 or C_{2+} products).[8] Product selectivity is still an issue, including the competition against the hydrogen evolution reaction (HER). Thus, it is necessary to develop affordable catalysts that suppress the HER and drive the CO_2RR efficiently at a low overpotential with high product selectivity. However, C_1 products are preferred over C_2 or C_{2+} compounds in most of the CO_2RR since the latter need to overcome a high activation energy barrier.[9] Methanol, in particular, is a crucial C_1 compound used as the primary precursor for producing bulk chemicals, including silicone and plastics.[10] Yet, the electrochemical conversion of CO_2 into methanol with high efficiency and selectivity is limited, demanding more investigation into new classes of catalysts.[10,11]

Single-atom catalysts (SACs)[12−16] are a novel class of emerging catalytic materials. Various nanostructured materials,

Received: August 29, 2023
Revised: November 3, 2023
Accepted: November 3, 2023

including graphene,[17,18] metal−organic frameworks (MOFs),[19−21] carbon nanotubes (CNTs),[22,23] and covalent organic frameworks (COFs)[24−26] have been exploited as the carbon support for synthesizing SACs. The carbon support provides a unique electronic structure along with high conductivity.[27] Recently, we demonstrated Cu- and Fe-based SACs using crystalline carbon nitride (PHI) as the carbon support by the cation-exchange method. Under mild conditions, via photocatalysis, PHI-derived Cu-SACs and Fe-SACs showed remarkable catalytic activity for methane oxidation to methanol (2900 μmol g^{-1}) and C−H bond oxidation reactions.[28,29] Due to their high unsaturated coordination, maximum atom utilization, distinctive electronic structure, and capacity to suppress HER, they have drawn expressive attention in CO_2RR.[30] Covalent triazine frameworks (CTFs),[31] of the typical COF[32] family, composed of strong covalent bonds, are another potential catalyst-supporting materials with similar properties.[33] Unlike MOFs, CTFs, and COFs can be synthesized with various heteroatoms (i.e., N, S, etc.) and conductive features. For example, a perylenediimide[34−36] (PDI)-incorporated CTF can provide high conductive and unique electronic properties for the whole system. Only a few attempts have been made to integrate PDI in the CTF,[37,38] and no reports have shown the significance of such frameworks in CO_2RR.

Despite the significant advancements in developing various photo- and electrocatalysts for CO_2RR,[39−50] SACs based on COFs and CTFs are scarce in the literature.[24,51−53] Moreover, the production of methanol with high selectivity remains limited.[10,11] Copper-based single-atom catalysts (Cu-SACs), in particular, are promising for the electrocatalytic conversion of CO_2 into hydrocarbons and alcohols with high product selectivity in an aqueous solution.[54−63] Thus, herein, we report CTF-Cu-SACs using PDI-incorporated CTFs as the conductive carbon support for CO_2RR. The CTF-Cu-SACs demonstrated high catalytic efficiency of converting CO_2 to methanol with an FE of 72.6% at 0.2 V vs RHE. While increasing the overpotential (0.0 to −0.4 V), CTF-Cu-SACs favored syngas (CO and H_2) production. The CTF-Cu-SACs maintained high stability for 24 h of continuous electrolysis. From this investigation, CTF-Cu-SACs pave the way to utilize PDI-incorporated CTFs as the sustainable conductive carbon support for next-generation SACs to be explored as potential electrocatalysts for CO_2RR by considering their structural designability for metal coordination and unique electronic features.

EXPERIMENTAL SECTION

Synthesis of PDI-CTF. The PDI-CTF was prepared according to the literature.[37] Briefly, melamine (5 mM) was mixed with 3,4,9,10-perylenetetracarboxylic acid anhydride (PTCDA, 5 mM). The resulting mixture was then ground in an agate mortar for 30 min. Following this, the resultant mixture was carefully transferred into an alumina crucible and exposed to a calcination process at a temperature of 325 °C for 4 h. This process occurred in an air atmosphere with a controlled heating rate of 5 °C per minute. Ultimately, the resulting particles were collected for subsequent usage.

Synthesis of CTF-Derived Cu-SACs (CTF-Cu-SACs). In a typical synthesis, PDI-CTF (0.3 g) and $Cu(OAC)_2{\cdot}2H_2O$ (0.03 g; 10 wt %) were ground in a silica mortar for 30 min to attain a homogeneous mixture. Subsequently, the mixture was annealed at 900 °C, 3 °C/min, for 4 h under N_2. After pyrolysis, the mixture was successfully leached at HCl (1 M) and HNO_3 (1 M) at 80 °C for 12 h each to remove metal nanoparticles or clusters, if any. Finally, the acid mixture was centrifuged at 8000 rpm for 10 min and thoroughly washed with water (Milli-Q), followed by drying at 80 °C for 12 h under a vacuum to obtain pure CTF-derived Cu-SACs (CTF-Cu-900). A similar strategy was used for synthesizing N-doped Cu-SACs (CTF-Cu-N-900) using melamine (1:10) as the nitrogen source. Metal-free pyrolyzed CTF (CTF-900) was also synthesized for comparison. The catalyst yield was calculated at ∼55 to 66%.

Characterizations. A Shimadzu diffractometer (XRD-6000) with a Cu Kα source (λ = 1.5418 Å) was used to record the results of a powder X-ray diffraction (PXRD) investigation in the 10 to 80° (1° min^{-1}) range. All samples underwent thermogravimetric analyses (TGA) using a TGA Q500 analyzer in a platinum pan with airflow rates of 40 mL min^{-1} for the sample and 60 mL min^{-1} for the reference separately. The temperature was increased at a rate of 10 °C per minute. Micromeritics equipment (ASAP 2020) was used to analyze the adsorption and desorption of nitrogen at 80 °C for 1 h. It was performed using the Brunauer−Emmett−Teller (BET) equation to determine the specific surface area (SSA). A confocal LabRAM micro-Raman system with a 532 nm laser was used to perform Raman spectroscopy. A high-performance EA 125 hemispherical analyzer was used for the X-ray photoelectron spectroscopy (XPS) analysis, and an operating pressure of 2×10^{-9} mbar was used in the ultrahigh vacuum chamber. The samples were exposed to monochromatic Al K radiation ($h\nu$ = 1486.6 eV). Scanning electron microscopy (SEM) and energy-dispersive X-ray spectroscopy (EDX) were carried out by using a JEOL JEM 2010 microscope with a tungsten filament. The samples were deposited by using carbon tape before analysis. Using an FEI JEOL-7800F, field-emission scanning electron microscopy (FE-SEM) was carried out. An FEI-TECNAI G2 F20 microscope was used to record high-angle annular dark-field scanning transmission electron microscopy (HAADF-STEM) and element mapping analysis (EDS) (200 kV). On an electrochemical workstation, linear sweep voltammetry (LSV) was captured (Autolab PGSTAT30, Metrohm). Liquid products were examined by ^{1}H NMR spectroscopy (600 MHz, AscendTM 600 Bruker) at 25 °C. The standard and reference combined D_2O containing dimethyl sulfoxide (DMSO; 5.0 mM) and TSPd4 (0.22 mM). For the ^{1}H NMR, the sample (540 μL) and the solution mentioned above (60 μL each) were combined. The ^{1}H NMR data were quantified by using the MestReNova program. Gas chromatography (GC Thermo CP-3800) was employed to find gaseous products. A carboxen 1010 plot capillary GC column (30 m × 0.32 mm, average thickness 15 μm) was used to separate the gaseous products of the CO_2 reduction on a GC instrument equipped with flame ionization (FID) and thermal conductivity (TCD) detectors and methanizers. Argon was used as the carrier gas.

Electrochemical Measurements. The electrochemical measurements were performed in a gastight H-type electrochemical cell equipped with a three-electrode system. All of the measurements were done at ambient temperature. A Nafion membrane was used to separate the anodic and cathodic compartments. Carbon paper (CP), platinum grid (Pt), and Ag/AgCl (3 M KCl) were used as the working (WE), counter (CE), and reference (RE) electrodes, respectively. All of the applied potentials were converted into RHE using the equation $E_{RHE} = E_{(Ag/AgCl)} + E^{\circ}_{(Ag/AgCl)} + (0.0591 \times pH)$.

Linear Sweep Voltammetry (LSV). LSV was performed in the potential window of 0 to −1.4 V vs Ag/AgCl (3 M) at a scan rate of 25 mV s^{-1} using 0.5 M KOH as an aqueous electrolyte. Before the measurement, N_2 (99.999%) or CO_2 (99.999%) was purged to saturate the 0.5 M KOH for 10 min by maintaining a flow of CO_2 throughout the measurement.

Catalyst Preparation. The pyrolyzed CTFs (CTF-900, CTF-Cu-900, and CTF-Cu-N-900) (2.0 mg) were dispersed in isopropyl alcohol (500 L), Milli-Q water (500 L), and Nafion (5%) (5.6 L) to create the catalytic ink. For even dispersion, the mixtures were sonicated for 20 min. After that, the CP (1 × 1 cm^2) was spray-coated with the catalytic ink, which was then dried for 12 h at room temperature.

Chronoamperometry (CA). To assess the electrochemical CO_2RR, CA was used. The cathodic compartment was initially purged with high-purity CO_2 (99.99%) for around 15 min. The CO_2RR was then

https://doi.org/10.1021/acs.energyfuels.3c03268
Energy Fuels XXXX, XXX, XXX−XXX

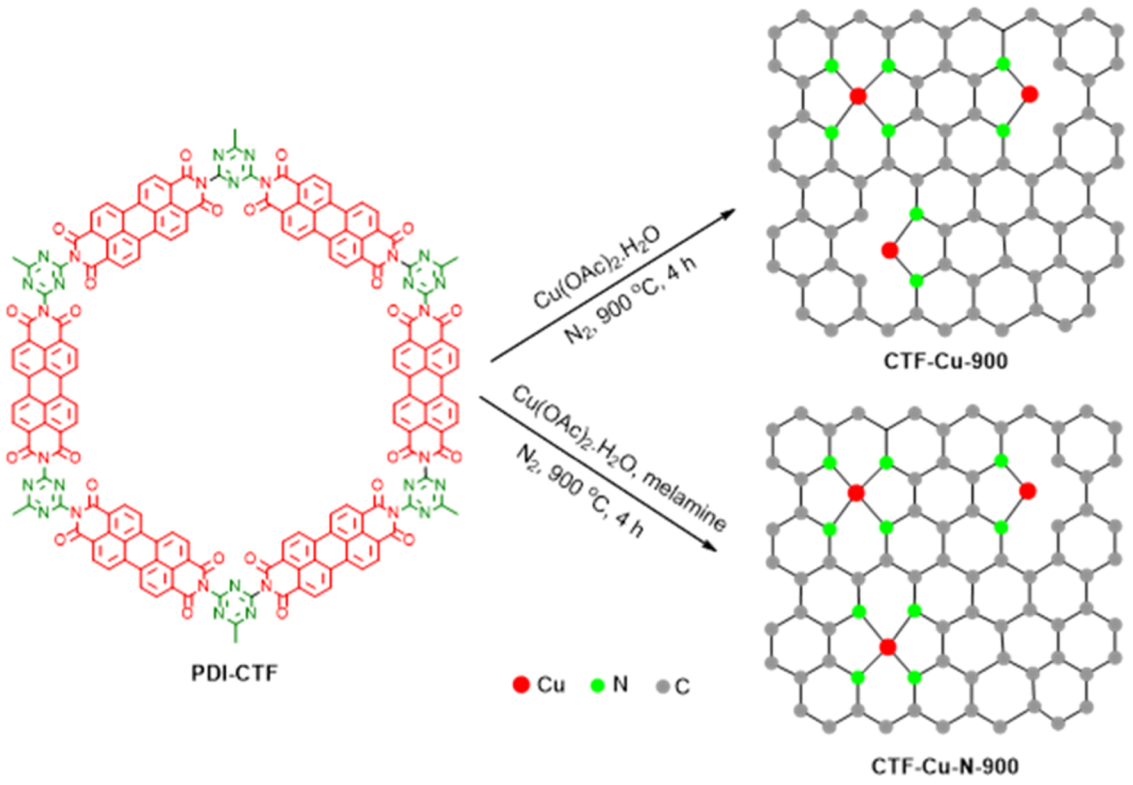

Figure 1. Schematic illustration for the synthesis of Cu-SACs on a PDI-CTF support.

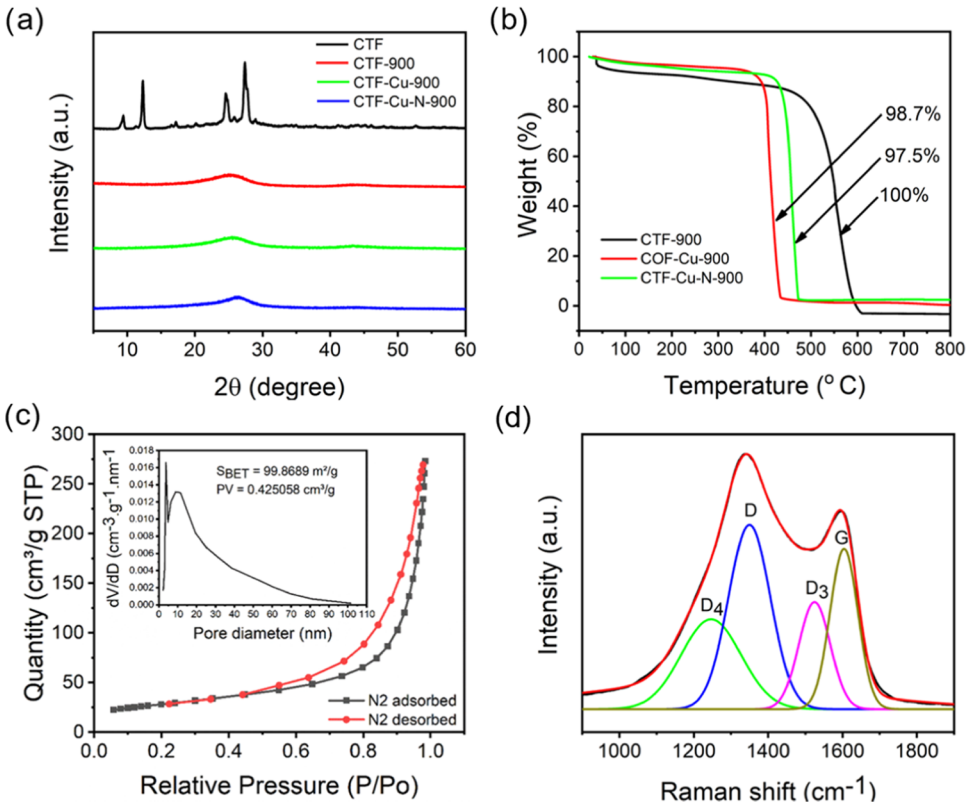

Figure 2. Characterization of CTF-Cu-SACs. (a) Representative XRD profiles of CTF, CTF-900, CTF-Cu-900, and CTF-Cu-N-900. (b) TGA profile of CTF-900, CTF-Cu-900, and CTF-Cu-N-900. (c) N_2 adsorption and desorption isotherms of CTF-Cu-N-900. Inset: Pore size distribution of CTF-Cu-N-900. (d) Raman spectrum of CTF-Cu-N-900.

performed for 30 min in a CO_2 environment. Following the process, the gaseous and liquid byproducts underwent GC and NMR spectroscopic analyses, respectively. All of the products' FEs were estimated using the equation given in the literature.[3]

https://doi.org/10.1021/acs.energyfuels.3c03268
Energy Fuels XXXX, XXX, XXX−XXX

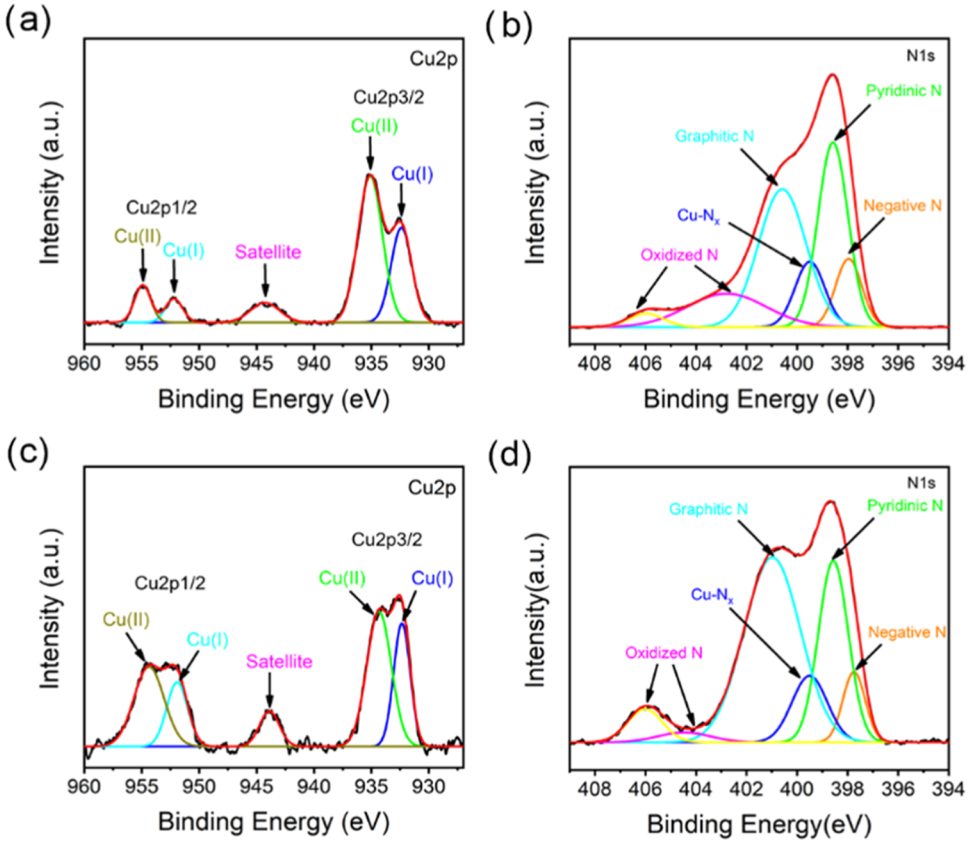

Figure 3. Surface composition of CTF-Cu-SACs. XPS high-resolution Cu 2p spectrum of CTF-Cu-N-900 (a) and CTF-Cu-900 (c). Respective XPS high-resolution N 1s spectrum of CTF-Cu-N-900 (b) and CTF-Cu-900 (d).

Electrochemical Surface Area (ECSA). ECSA was measured using cyclic voltammetry (CV) at the solid−liquid interface by measuring the double-layer capacitance. The measurement was carried out in a nonfaradaic potential range of 0.0−0.5 V vs Ag/AgCl (3 M) at the scan rates ranging from 10 to 50 mV s^{-1} to construct a plot of the charging current density differences against the scan rate at a fixed potential of 0.25 V. ECSA was carried out according to the literature.[3,64]

Electrical Impedance Spectroscopy (EIS). Glassy carbon, platinum, and Ag/AgCl were used as the working, counter, and reference electrodes, respectively, to record EIS on an Autolab (PGSTAT302N). The settings for all of the analyses were CO_2-saturated. All of the catalysts had a frequency range of 0.001−10^5 Hz and an amplitude of 0.005 V.

RESULTS AND DISCUSSION

Synthesis and Characterization. As depicted in Figure 1, CTF-Cu-SACs (CTF-Cu-900 and CTF-Cu-N-900) were synthesized using PDI-CTF as the conductive carbon support. CTF-Cu-900 was produced by pyrolyzing PDI-CTF[37] in the presence of $Cu(OAC)_2.2H_2O$ at 900 °C for 4 h at a heating rate of 3 °C/min in a N_2 environment. CTF-Cu-SACs with additional N-doping (CTF-Cu-N-900) were synthesized using melamine as the N-donating agent. Notably, N-doping on carbonaceous frameworks increases the stability of Cu atoms by preventing their aggregation with surrounding atoms.[19] We also synthesized the metal-free carbon substrate CTF-900 for comparison in the absence of $Cu(OAC)_2{\cdot}H_2O$. Following pyrolysis, all samples were treated for 12 h at 80 °C with 1 M HCl and 1 M HNO_3 to remove Cu nanoparticles (CuNPs) or clusters adsorbed on the framework's edge.[19]

The XRD profile of CTF-900, CTF-Cu-900, and CTF-Cu-N-900 exhibited a broad peak at 26.4 and 44.1°, attributed to the planes (002) and (100) of the graphitic structure, respectively.[11,13] Bare PDI-CTF shows clear crystalline diffraction peaks (Figure 2a). With CTF-Cu-900 and CTF-Cu-N-900, no apparent crystalline peaks were seen, indicating the absence of any metal nanoparticles or clusters.[11,13] TGA analysis was used to determine the thermal characteristics of CTF-900, CTF-Cu-900, and CTF-Cu-N-900 (Figure 2b). The weight loss for CTF-Cu-900 and CTF-Cu-N-900 was 98.7 and 97.5%, respectively, at the highest temperature (800 °C). However, when the maximum temperature was applied, the metal-free CTF-900 catalyst lost (100%) weight utterly. The catalysts' negligible weight loss compared to the metal-free CTF-900 catalyst confirms the evidence that metal atoms are present in CTF-Cu-900 and CTF-Cu-N-900. Of all of the samples examined, CTF-Cu-N-900 had the lowest weight loss (97.5%), which could be attributed to the additional N-doping increasing the amount of Cu-coordinated with the N-ligand in the carbon matrix.

The surface area and pore volume of the CO_2RR are considered crucial attributes as they enhance its catalytic activity by providing a more significant number of catalytic sites. The catalysts CTF-900 and CTF-Cu-900 yielded BET surface areas of about 13.7 and 8.9 m^2/g, respectively, as shown in Figure S1a,b. Additionally, it was determined that the pore volumes of CTF-900 and CTF-Cu-900 were about 0.04 and 0.05 cm^3/g, respectively, as seen in Figure S1a,b. On the other hand, it was observed that the N-doped CTF-Cu-N-900 exhibited the highest BET surface area and pore volume among the samples, with values of around 99.8689 m^2/g and

https://doi.org/10.1021/acs.energyfuels.3c03268
Energy Fuels XXXX, XXX, XXX−XXX

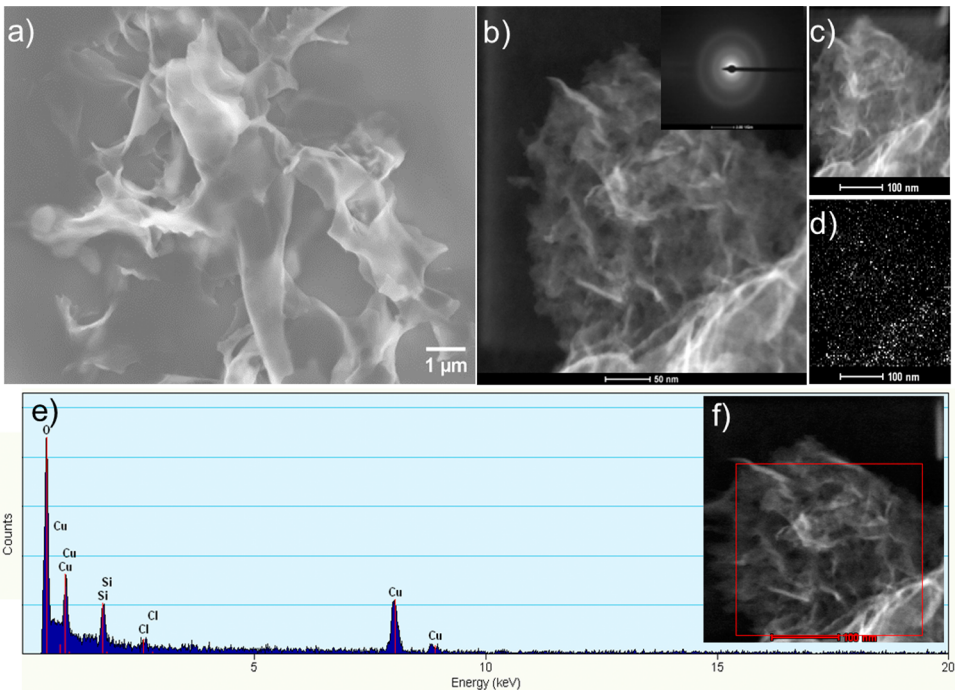

Figure 4. Morphology of CTF-Cu-SACs. (a) FE-SEM patterns of CTF-Cu-N-900. (b) HAAD-STEM image of CTF-Cu-N-900 (the inset shows the SAED pattern). (c, d) HAADF-STEM image and representative EDS mapping of CTF-Cu-N-900 (the white dot represents an isolated copper atom). (e, f) EDS graph from the selected region of CTF-Cu-N-900.

0.42 cm^3/g, respectively (Figure 2c and inset). It suggests that the metal atom experiences stabilization while the N-dopants contribute to an enlargement in the surface area.

Moreover, Raman spectra were obtained to clarify the structure of CTF-Cu-SACs, which may be deconvoluted into four distinct peaks (Figures 2d and S2). For instance, CTF-Cu-N-900 (Figure 2d) showed peaks at around 1244 and 1350 cm^{-1} attributed to the sp^3 phase of a polyene-like structure (D4-band) and the carbon matrix. A band around 1524 cm^{-1} may be related to the carbon matrix's Cu-Nx coordination or the amorphous sp^2 phase (D3 band). The in-plane vibration of the carbon atoms in the sp^2 electronic arrangement is attributed to a band at about 1604 cm^{-1}.[19]

The chemical compositions of CTF-900, CTF-Cu-900, and CTF-Cu-N-900 are revealed by XPS analysis. The prominent peaks in the XPS survey spectra of CTF-Cu-900 and CTF-Cu-N-900 were carbon (C 1s), nitrogen (N 1s), and oxygen (O 1s), respectively, at 284.8, 400, and 530.6 eV. (Figure S3a−c). The coordination of H_2O and O_2 with Cu single atoms to achieve a whole coordination sphere is likely the cause of oxygen's presence in CTF-Cu-SACs.[65] The presence of Cu 2p with mixed valence states like Cu(I) (932.4 and 952.1 eV) and Cu(II) (934.9 and 954.8 eV) as well as the satellite peaks in the range of 942 to 948 eV, which could be attributed to the Cu-Nx coordination of Cu(I) and Cu(II) valence states, was demonstrated in the high-resolution spectrum by CTF-Cu-N-900 and CTF-Cu-900 (Figure 3a,c). It is in line with past reports on N-doped Cu-SACs in a positive way.[19,66−68] Moreover, due to peak intensity variation, N-doping to the CTF-Cu-SACs significantly affected the Cu(I)/Cu(II) proportion. Due to the high amount of N-source, N-doped CTF-Cu-N-900, for example, showed intense peaks for the Cu (II) over Cu (I) state, indicating that the catalyst mainly comprises $Cu-N_4$ valence states rather than $Cu-N_2$ valence states. In contrast, CTF-Cu-900 exhibited a high intensity for the Cu(I) state, ascribed to the $Cu-N_2$ valence states. Six suitable peaks were deconvoluted from the high-resolution N 1s spectra of CTF-Cu-N-900 and CTF-900 (Figure 3b,d). Pyridinic-N and graphitic-N states are linked to 398.4 and 400.8 eV peaks.[19,66−68] Importantly, the Cu-Nx coordination in CTF-Cu-SACs may be attributed to a peak at 399.4 eV.[19,66−68] Moreover, negative-N and oxidized-N were seen at energies of 397.9 and 403−406 eV.[28] The catalyst CTF-Cu-N-900 displays a substantially higher N-peak than other catalysts, indicating that the N atoms in the catalyst were added through additional N-doping (Figure S3c). The survey spectrum of the metal-free CTF-900 verifies that there are no metal peaks, as expected (Figure S3a). Our findings showed that the N and Cu atoms dominate the carbon matrix, suggesting that their strong coordination in mixed valence states makes them a promising option for electrocatalysis.

CTF-900 and CTF-Cu-900 both exhibited a foam-like structure in field-emission scanning electron microscopy (FE-SEM) images (Figure S4a,b), whereas CTF-Cu-N-900 was made of an ultrathin sheet-like structure (Figure 4a). The carbon matrix contains atoms of carbon (C), nitrogen (N), oxygen (O), and copper (Cu), according to SEM-EDS elemental mapping (Figure S5). CTF-Cu-N-900 was found to have a sheet-like structure in HAAD-STEM analysis (Figure 4b). Remarkably, even at high magnification (Figures 4b and S6a,b), neither copper nanoparticles (CuNPs) nor clusters are seen in the HAAD-STEM pattern of CTF-Cu-N-900, suggesting the presence of copper single atoms.[19] Moreover, the selected area electron diffraction (SAED) pattern revealed only the carbon diffraction fringe (Figure 4b, inset). This observation agrees with the CTF-Cu-SACs' XRD pattern, with no distinctive peaks connected to CuNPs or clusters. HAAD-EDS mapping of CTF-Cu-N-900 demonstrated the presence of extensively scattered copper single atoms in the carbon matrix (Figure 4c,4d). Also, the chosen region's HAAD-EDS

https://doi.org/10.1021/acs.energyfuels.3c03268
Energy Fuels XXXX, XXX, XXX−XXX

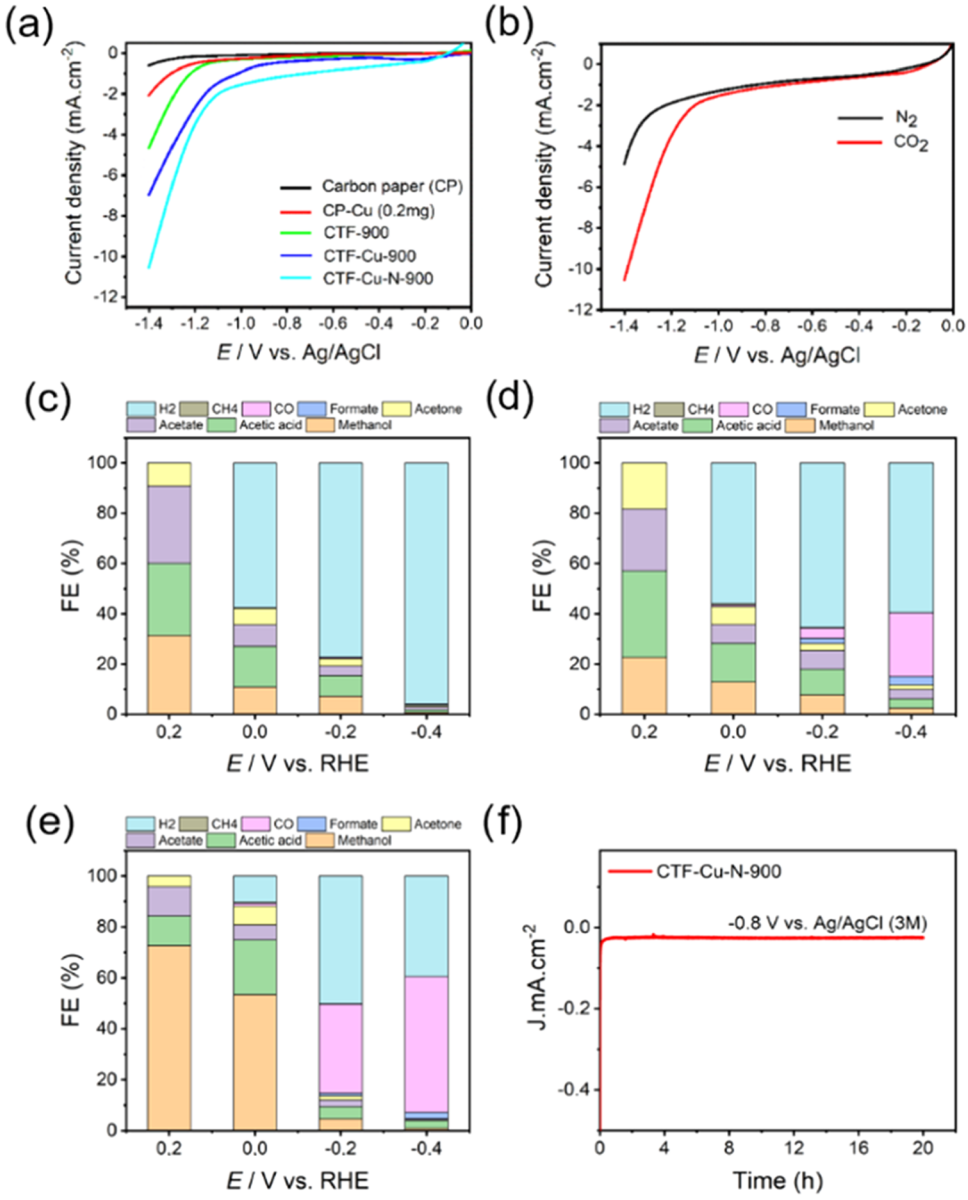

Figure 5. Electrochemical CO_2 conversion of CTF-Cu-SACs. (a) LSV curves were recorded in a CO_2-saturated 0.5 M KOH solution of CTF-Cu-N-900, CTF-Cu-900, CTF-900, and reference electrodes. (b) LSV curves were recorded in a N_2- and a CO_2-saturated 0.5 M KOH solution of CTF-Cu-N-900. Faradaic efficiencies of all products at the potential range of 0.2 to −0.4 V vs RHE for CTF-900 (c), CTF-Cu-900 (d), and CTF-Cu-N-900 (e). (f) The stability of CTF-Cu-N-900 for 20 h at −0.8 V vs Ag/AgCl (3 M).

graph amply supports the existence of the Cu atom in CTF-Cu-N-900 (Figure 4e,f).

Electrochemical CO_2 Conversion. The electrocatalytic CO_2RR performance of CTF-Cu-SACs was tested in a gastight H-type electrochemical cell with a three-electrode configuration, with 0.5 M KOH from 0.0 V to −1.4 V vs Ag/AgCl under N_2- or CO_2-saturated circumstances. CTF-Cu-N-900 produced a current density (~11 mA cm^{-2}) in linear sweep voltammetry (LSV) higher than that of the other catalysts (Figure 5a). A significantly greater current density of CTF-Cu-N-900 under CO_2-saturated electrolytic conditions (Figure 5b) than N_2-saturated conditions (Figure 5b) suggests its superior catalytic performance in CO_2RR.[24] Also, the extra N-doping to the CTF-Cu-SACs demonstrated tremendous relevance in raising the current densities, a crucial aspect for the electrocatalytic CO_2RR. N-doping into the carbon matrix creates additional defects to anchor single metal sites and tune the electrical structure of the entire system. Also, the low Ohmic resistance of KOH, as an electrolyte, enhances the current density compared to the other electrolytes.[69]

Methanol, acetic acid, acetate, and acetone were all detected in trace amounts in CO_2RR using the metal-free catalyst CTF-900 at the lower overpotential (0.2 V vs RHE). However, at the upper range of overpotentials (0.0 to −0.4 V versus RHE), a significant HER was noted (Figure 5c). The primary products of the metal-doped catalysts CTF-Cu-900 and CTF-Cu-N-900, on the other hand, ranged from 0.2 to −0.4 V vs RHE and were methanol, CO, and H_2 (Figure 5d,5e). For instance, CTF-Cu-900 favored syngas generation with FEs of 25.2% (CO) and 59.5% (H_2) at a higher overpotential (−0.4 V vs RHE) and CO_2 to methanol with an FE of 22.6% at a lower overpotential (0.2 V vs RHE). Notably, N-doped CTF-Cu-N-900 showed excellent catalytic performance in the conversion of CO_2 into methanol with an FE of 72.6% at a relatively low

https://doi.org/10.1021/acs.energyfuels.3c03268
Energy Fuels XXXX, XXX, XXX−XXX

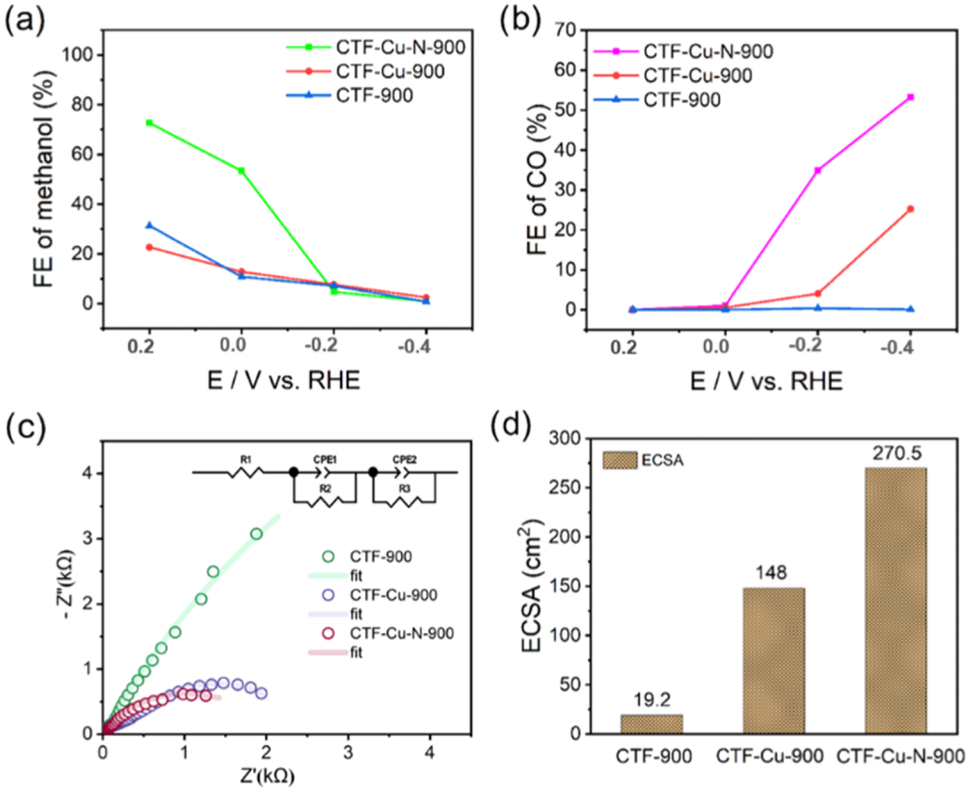

Figure 6. Faradaic efficiencies of methanol (a) and CO (b) at the potential range of 0.2 to −0.4 V vs RHE for CTF-SACs. (c) EIS spectra of CTF-SACs catalysts under CO_2-saturated conditions in the 0.001−10^5 Hz frequency range with an AC amplitude of 0.005 V. (d) ECSA of CTF-SACs under CO_2-saturated conditions from 10 to 50 mV s^{-1}.

overpotential of 0.2 V vs RHE (Figure 6a). The FE of methanol steadily dropped as the overpotential increased from 0.2 to −0.4 V vs RHE. Still, the FE of CO and H_2 dramatically increased, reaching their highest values of 53.2 and 39.5%, respectively, at −0.4 V vs RHE (Figure 6b). Besides, all of the three catalysts yield acetic acid, acetate, acetone, and methane as trace amounts throughout the potential range (Figure 5c−e). Moreover, a negligible formate production was observed only at a higher overpotential at −0.4 V (Figure 5e). Overall, it shows that at 0.2 V vs RHE, the N-doped CTF-Cu-N-900 produces the maximum FE of methanol (72.6%).

As discussed in earlier reports, C_1 molecules (CO and formic acid) were the primary products during most of the CO_2RR using Cu-based M−N−C catalysts.[54−63] CTF-Cu-SACs could convert CO_2 into methanol in an aqueous solution with an FE of 72.6% and a partial current density of ∼−11 mA cm^{-2}. This catalytic performance of CTF-Cu-SACs is superior to that of the previously reported state-of-the-art catalysts based on Cu for CO_2 reduction to methanol in electrocatalysis (Table S1).

The proposed hypothesis posits that in the reaction pathway of the CO_2RR, carbon monoxide (CO) serves as an intermediate species, facilitating the formation of C_1 or C_{2+} molecules by proton and electron transfer processes. The relatively low binding energy of *CO intermediates on the catalyst surface enhances the removal of CO as a product. At the same time, the firmly adsorbed *CO species undergo further reduction processes, leading to the formation of methanol.[11] Also, it is worth noting that copper nanoparticles (CuNPs) or clusters can potentially promote the formation of multi-carbon (C_2 or C_{2+}) products. It is due to the proximity of *CO intermediates, which enables C−C coupling within a carbonaceous matrix.[54,70−73] Nevertheless, it is widely observed that single-atom catalysts (SACs) tend to result in the formation of C_1 compounds. It might be attributed to the greater interatomic distance between the metal atoms, which hinders the interaction between carbon atoms (C−C interaction).[54−63] Therefore, it can be inferred that the preference of our catalysts for methanol is mainly due to the presence of a uniform Cu-Nx structure.

Catalyst stability is influenced by structural modifications, variations in electrolyte pH, and the presence of solution contaminants, acting synergistically.[19] To assess the stability of CTF-Cu-N-900 under CO_2RR conditions, we conducted a 20 h test. The results showed that continuous electrolysis at −0.8 V vs Ag/AgCl (3 M) did not cause a significant change in the current density, indicating its excellent catalytic stability (Figure 5f).

The electrical conductivities of catalysts CTF-900, CTF-Cu-900, and CTF-Cu-N-900 were investigated by electrochemical impedance spectroscopy (EIS). In contrast to CTF-Cu-900 and CTF-900, as shown in Figure 6c, N-doped CTF-Cu-N-900 had the lowest charge transfer resistance, which is advantageous for the CO_2RR because it enhances electronic contact.

Based on the calculations performed, it can be observed that CTF-900, CTF-Cu-900, and CTF-Cu-N-900 exhibit electrochemical surface areas (ECSA) of approximately 19.2, 148.0, and 270.5 cm^2, respectively, as depicted in Figure 6d. Also, this investigation revealed that the nonfaradaic potential exhibited pseudocapacitance values of around 0.77, 5.92, and 10.82 mF cm^{-2} for CTF-900, CTF-Cu-900, and CTF-Cu-N-900, respectively (see Figure 7a−d). The observed high electro-

https://doi.org/10.1021/acs.energyfuels.3c03268
Energy Fuels XXXX, XXX, XXX−XXX

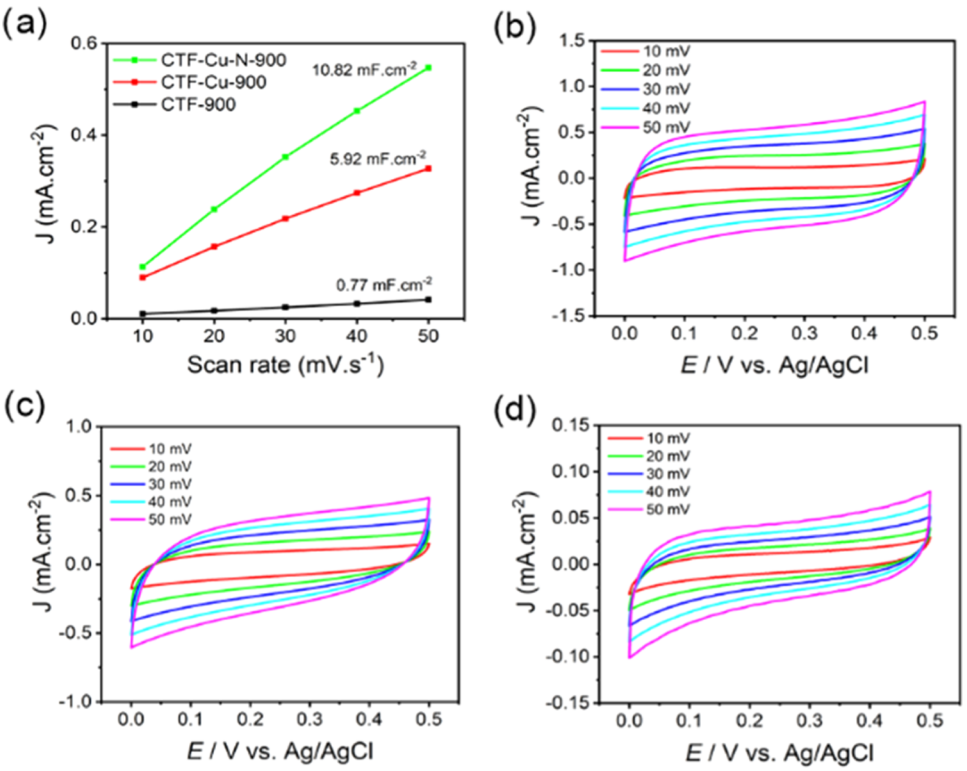

Figure 7. ECSA of CTF-SACs. (a) Pseudocapacitance of CTF-900, CTF-Cu-900, and CTF-Cu-N-900 at 0.25 V vs Ag/AgCl from 10 to 50 mV s^{-1}. Respective CV curves of CTF-Cu-N-900 (b), CTF-Cu-900 (c), and CTF-900 (d) in the range of nonfaradaic potential ranging from 0 to 0.5 V vs Ag/AgCl.

chemical surface area (ECSA) of CTF-Cu-N-900 can be attributed to its hierarchical porous structure, which possesses a significant surface area and pore volume. This characteristic is likely responsible for providing more active sites for the CO_2 reduction reaction (CO_2RR). The observed results are consistent with the superior catalytic performance of CTF-Cu-N-900 in the CO_2 reduction reaction (CO_2RR) compared with other prepared catalysts. Hence, this study's observed increase in the CO_2RR efficiency, particularly for the CTF-Cu-N-900 catalyst, can be attributed primarily to the synergistic impact of the highly conductive pyrolyzed CTF and N-chelating ligands. This synergy facilitates rapid intermolecular ion and charge transfer, resulting in abundant active sites for the reaction. Furthermore, incorporating a PDI-derived CTF inside the carbon matrix has significantly improved its electric conductivity. This enhancement facilitates electron transmission and provides highly efficient active sites for the electrochemical reduction of carbon dioxide (CO_2RR).

CONCLUSIONS

In conclusion, it has been shown that a highly conductive PDI-CTF can serve as a carbon support for the synthesis of Cu-SACs. With 72.6% of FE and a low overpotential (0.2 V vs RHE), the CTF-Cu-SACs have demonstrated their efficiency as electrocatalysts for converting CO_2 into methanol. On the other hand, when the overpotential was increased from 0.2 to −0.4 V vs RHE, CTF-Cu-SACs favored syngas (CO and H_2) generation. Moreover, at −0.4 V vs RHE, a large amount of CO with an FE of 53.2% was produced. We also discovered that by stabilizing the Cu atom and supplying more catalytically active sites in the CO_2RR, the extra N-doping to the PDI-CTF significantly influences the catalytic performance of CTF-Cu-SACs. This product generation may be primarily attributable to the abundant Cu active sites with a single atom in the carbonaceous matrix of PDI-CTF. Therefore, PDI-based CTF-Cu-SACs are a promising candidate for a heterogeneous catalyst because of their simple synthesis, superior electronic characteristics, and highly monodispersed single atoms.

ASSOCIATED CONTENT

Supporting Information

The Supporting Information is available free of charge at https://pubs.acs.org/doi/10.1021/acs.energyfuels.3c03268.

BET surface analysis of CTF-Cu-SACs (Figure S1); Raman spectrum of CTF-Cu-900 (Figure S2); surface composition of CTF-Cu-SACs (Figure S3); FE-SEM images of CTF-Cu-SACs (Figure S4); SEM-EDS mapping of CTF-Cu-SACs (Figure S5); HAAD-STEM images of CTF-Cu-SACs (Figure S6), and electrocatalytic performances of Cu-based catalysts for the production of methanol (Table S1) (PDF)

AUTHOR INFORMATION

Corresponding Authors

Sebastian Raja − *National Nanotechnology Laboratory for Agribusiness (LNNA), Embrapa Instrumentação, São Carlos, SP 13560-970, Brazil; Department of Chemistry, Federal University of São Carlos (UFSCar), São Carlos, SP 13565-905, Brazil; Department of Physical Chemistry and Technology of Polymers, Silesian University of Technology, Gliwice 44-100, Poland; Centre for Organic and Nanohybrid Electronics, Silesian University of Technology, Gliwice 44-100, Poland;* orcid.org/0000-0003-4648-5624; Email: sebastianrajaorg@gmail.com

https://doi.org/10.1021/acs.energyfuels.3c03268
Energy Fuels XXXX, XXX, XXX−XXX

Caue Ribeiro − *National Nanotechnology Laboratory for Agribusiness (LNNA), Embrapa Instrumentação, São Carlos, SP 13560-970, Brazil; Department of Chemistry, Federal University of São Carlos (UFSCar), São Carlos, SP 13565-905, Brazil;* orcid.org/0000-0002-8908-6343; Email: caue.ribeiro@embrapa.br

Authors

Gelson T. S. T. da Silva − *National Nanotechnology Laboratory for Agribusiness (LNNA), Embrapa Instrumentação, São Carlos, SP 13560-970, Brazil; Department of Chemistry, Federal University of São Carlos (UFSCar), São Carlos, SP 13565-905, Brazil;* orcid.org/0000-0001-9448-1455

Eduardo A. Reis − *National Nanotechnology Laboratory for Agribusiness (LNNA), Embrapa Instrumentação, São Carlos, SP 13560-970, Brazil; São Carlos Institute of Chemistry, University of São Paulo, São Carlos 13566-590, Brazil*

Jean C. da Cruz − *National Nanotechnology Laboratory for Agribusiness (LNNA), Embrapa Instrumentação, São Carlos, SP 13560-970, Brazil*

Anelisse Brunca Silva − *Department of Chemistry, Federal University of São Carlos (UFSCar), São Carlos, SP 13565-905, Brazil*

Marcelo B. Andrade − *São Carlos Institute of Physics, University of São Paulo, São Carlos 3563-120, Brazil; Physics Department, Federal University of Ouro Preto, Ouro Preto, MG 35400-000, Brazil;* orcid.org/0000-0001-9137-8831

Govindasami Periyasami − *Department of Chemistry, College of Science, King Saud University, Riyadh 11451, Saudi Arabia;* orcid.org/0000-0003-1181-1645

Perumal Karthikeyan − *Department of Chemistry and Biochemistry, Ohio State University, Columbus, Ohio 43210, United States*

Igor F. Perepichka − *Department of Physical Chemistry and Technology of Polymers, Silesian University of Technology, Gliwice 44-100, Poland; Centre for Organic and Nanohybrid Electronics, Silesian University of Technology, Gliwice 44-100, Poland;* orcid.org/0000-0001-6672-3103

Lucia Helena Mascaro − *Department of Chemistry, Federal University of São Carlos (UFSCar), São Carlos, SP 13565-905, Brazil;* orcid.org/0000-0001-6908-1097

Complete contact information is available at: https://pubs.acs.org/10.1021/acs.energyfuels.3c03268

Notes

The authors declare no competing financial interest.

■ ACKNOWLEDGMENTS

Dr. Raja thanks CAPES (Proc. No. 88887.575987/2020-00) for financial support in the scheme of PrInt. The authors are grateful to the Ministry of Science, Technology, and Innovation (through SisNANO Program—National System of Laboratories in Nanotechnology), FINEP (Process 01.17.0021.00 and 01.22.0179.00), National Council for Scientific and Technological Development (CNPq; Grants #442575/2019-0, #152607/2022-6, #311769/2022-5, and #406156/2022-0) and FAPESP (Grants #2018/01258-5, #2022/10255-5, #2017/11986-5, and # #2013/07296-2) for financial support. The authors are also grateful to CAPES (Coordination for the Improvement of Higher Education Personnel—Finance Code 001) and the Brazilian Nanotechnology Laboratory for Research in Energy and Materials (LNNano) for facilities. Dr. Periyasami thanks for funding from "Ministry of Education" in Saudi Arabia (IFKSUOR3-572-1). The authors also thank Shell and the strategic importance of the support given by ANP (Brazil's National Oil, Natural Gas, and Biofuels Agency) through the R&D levy regulation. They also acknowledge funding from EU's Horizon 2020 ERA-Chair project ExCEED (Grant Agreement No. 952008).

■ REFERENCES

(1) Raja, S.; Mattoso, L. H. C. Functionalized Polymer-Based Composite Photocatalysts. In *Green Photocatalysts. Environmental Chemistry for a Sustainable World*; Naushad, M.; Rajendran, S.; Lichtfouse, E., Eds.; Springer: Cham, 2020; Vol. *34*, pp 167−188.

(2) Nogueira, A. E.; Da Silva, G. T. S. T.; Oliveira, J. A.; Lopes, O. F.; Torres, J. A.; Carmo, M.; Ribeiro, C. CuO Decoration Controls Nb_2O_5 Photocatalyst Selectivity in CO_2 Reduction. *ACS Appl. Energy Mater.* **2020**, *3*, 7629−7636.

(3) Dias, E. H.; Da Silva, G. T. S. T.; Da Cruz, J. C.; Ribeiro, C. One-Pot Solvothermal Synthesis of Carbon Black-Supported CuO for Catalysis of CO_2 Electroreduction. *ChemElectroChem* **2022**, *9*, No. e202200206.

(4) Wang, Y.; He, D.; Chen, H.; Wang, D. Catalysts in electro-, photo- and photoelectrocatalytic CO_2 reduction reactions. *J. Photochem. Photobiol., C* **2019**, *40*, 117−149.

(5) Medvedev, J. J.; Tracey, C.; Engelhardt, H.; Steksova, Y.; Krivoshapkin, P.; Krivoshapkina, E.; Klinkova, A. Hands-on Electrochemical Reduction of CO_2: Understanding Electrochemical Principles through Active Learning. *J. Chem. Educ.* **2022**, *99*, 1036−1043.

(6) Souza, F. L.; Lopes, O. F.; Santos, E. V.; Ribeiro, C. Promoting CO_2 electroreduction on boron-doped diamond electrodes: Challenges and trends. *Curr. Opin. Electrochem.* **2022**, *32*, No. 100890.

(7) Yang, C.; Wang, Y.; Qian, L.; Al-Enizi, A. M.; Zhang, L.; Zheng, G. Heterogeneous Electrocatalysts for CO_2 Reduction. *ACS Appl. Energy Mater.* **2021**, *4* (2), 1034−1044.

(8) Chan, K. A few basic concepts in electrochemical carbon dioxide reduction. *Nat. Commun.* **2020**, *11*, No. 5954.

(9) Jaster, T.; Gawel, A.; Siegmund, D.; Holzmann, J.; Lohmann, H.; Klemm, E.; Apfel, U. Electrochemical CO_2 reduction toward multicarbon alcohols - The microscopic world of catalysts & process conditions. *iScience* **2022**, *25*, No. 104010.

(10) Liu, Y.; Li, F.; Zhang, X.; Ji, X. Recent progress on electrochemical reduction of CO_2 to methanol. *Curr. Opin. Green Sustainable Chem.* **2020**, *23*, 10−17.

(11) Yang, H.; Wu, Y.; Li, G.; Lin, Q.; Hu, Q.; Zhang, Q.; Liu, J.; He, C. Scalable Production of Efficient Single-Atom Copper Decorated Carbon Membranes for CO_2 Electroreduction to Methanol. *J. Am. Chem. Soc.* **2019**, *141*, 12717−12723.

(12) Ji, S.; Chen, Y.; Wang, X.; Zhang, Z.; Wang, Z. D. W.; Li, Y. Chemical Synthesis of Single Atomic Site Catalysts. *Chem. Rev.* **2020**, *120*, 11900−11955.

(13) Yang, H.; Shang, L.; Zhang, Q.; Shi, R.; Waterhouse, G. I. N.; Gu, L.; Zhang, T. A universal ligand mediated method for large scale synthesis of transition metal single atom catalysts. *Nat. Commun.* **2019**, *10*, No. 4585.

(14) Li, F.; Hong, S.; Wu, T.; Li, X.; Masa, J.; Soo, Y.; Sun, Z. Atomically Dispersed Nickel Sites for Selective Electroreduction of CO_2. *ACS Appl. Energy Mater.* **2019**, *2*, 8836−8842.

(15) Hung, S.-F.; Xu, A.; Wang, X.; Li, F.; Hsu, S.; Li, Y.; Wicks, J.; González Cervantes, E.; Rasouli, A. S.; Li, Y. C.; Luo, M.; Nam, D.; Wang, N.; Peng, T.; Yan, Y.; Lee, G.; Sargent, E. H. A metal-supported single-atom catalytic site enables carbon dioxide hydrogenation. *Nat. Commun.* **2022**, *13*, No. 819.

(16) Bai, X.; Zhao, X.; Zhang, Y.; Ling, C.; Zhou, Y.; Wang, J.; Liu, Y. Dynamic Stability of Copper Single-Atom Catalysts under Working Conditions. *J. Am. Chem. Soc.* **2022**, *144*, 17140−17148.

(17) Hu, C.; Mu, Y.; Bai, S.; Yang, J.; Gao, L.; Cheng, S.; Mi, S.; Qiu, J. Polyvinyl pyrrolidone mediated fabrication of Fe, N-codoped porous carbon sheets for efficient electrocatalytic CO_2 reduction. *Carbon* **2019**, *153*, 609−616.
(18) Zhang, H.-n.; Wang, H.; Jia, S.; Chang, Q.; Li, N.; Li, Y.; Shi, X.; Li, Z.; Hu, S. CoN_4 active sites in a graphene matrix for the highly efficient electrocatalysis of CO_2 reduction. *Carbon* **2022**, *37*, 734−742.
(19) Guan, A.; Chen, Z.; Quan, Y.; Peng, C.; Wang, Z.; Sham, T.; Yang, C.; Ji, Y.; Qian, L.; Xu, X.; Zheng, G. Boosting CO_2 Electroreduction to CH_4 *via* Tuning Neighboring Single-Copper Sites. *ACS Energy Lett.* **2020**, *5*, 1044−1053.
(20) Li, X.; Zhu, Q. MOF-based materials for photo- and electrocatalytic CO_2 reduction. *EnergyChem* **2020**, *2*, No. 100033.
(21) Rayer, A. V.; Reid, E.; Kataria, A.; Luz, I.; Thompson, S. J.; Lail, M.; Zhou, J.; Soukri, M. Electrochemical carbon dioxide reduction to isopropanol using novel carbonized copper metal organic framework derived electrodes. *J. CO_2 Util.* **2020**, *39*, No. 101159.
(22) Zou, X.; Ma, C.; Li, A.; Gao, Z.; Shadike, Z.; Jiang, K.; Zhang, J.; Huang, Z.; Zhu, L. Nanoparticle-Assisted Ni-Co Binary Single-Atom Catalysts Supported on Carbon Nanotubes for Efficient Electroreduction of CO2 to Syngas with Controllable CO/H2 Ratios. *ACS Appl. Energy Mater.* **2021**, *4*, 9572−9581.
(23) Wang, M.; Cai, Z.; Zhang, B.; Yang, K.; Shou, T.; Bernards, M. T.; Xie, P.; He, Y.; Shi, Y. Electrochemical Reduction of CO_2 on Copper-Based Electrocatalyst Supported on MWCNTs with Different Functional Groups. *Energy Fuels* **2022**, *36*, 5833−5842.
(24) Wang, R.; Yuan, Y.; Bang, K.; Kim, Y. Single-Atom Catalysts on Covalent Organic Frameworks for CO_2 Reduction. *ACS Mater. Au* **2023**, *3*, 28−36.
(25) Hasija, V.; Patial, S.; Raizada, P.; Khan, A. A. P.; Asiri, A. M.; Le, Q. V.; Nguyen, V.; Singh, P. Covalent organic frameworks promoted single metal atom catalysis: Strategies and applications. *Coord. Chem. Rev.* **2022**, *452*, No. 214298.
(26) Li, C.; Ju, W.; Vijay, S.; Timoshenko, J.; Mou, K.; Cullen, D. A.; Yang, J.; Wang, X.; Pachfule, P.; Brückner, S.; Jeon, H. S.; Haase, F. T.; Tsang, S.; Rettenmaier, C.; Chan, K.; Cuenya, B. R.; Thomas, A.; Strasser, P. Covalent Organic Framework (COF) Derived Ni-N-C Catalysts for Electrochemical CO_2 Reduction: Unraveling Fundamental Kinetic and Structural Parameters of the Active Sites. *Angew. Chem., Int. Ed.* **2022**, *61*, No. e202114707.
(27) Yang, Y.; Yang, Y.; Pei, Z.; Wu, K.; Tan, C.; Wang, H.; Wei, L.; Mahmood, A.; Yan, C.; Dong, J.; Zhao, S.; Chen, Y. Recent Progress of Carbon-Supported Single-Atom Catalysts for Energy Conversion and Storage. *Matter* **2020**, *3*, 1442−1476.
(28) Da Silva, M. A. R.; Gil, J. C.; Tarakina, N. V.; Da Silva, G. T. S. T.; Filho, J. B. G.; Krambrock, K.; Antonietti, M.; Ribeiro, C.; Teixeira, I. F. Selective methane photooxidation into methanol under mild conditions promoted by highly dispersed Cu atoms on crystalline carbon nitrides. *Chem. Commun.* **2022**, *58*, 7419−7422.
(29) da Silva, M. A. R.; Silva, I. F.; Xue, Q.; Lo, B. T. W.; Tarakina, N. V.; Nunes, B. N.; Adlerf, P.; Sahoo, S. K.; Bahnemann, D. W.; Lopez-Salas, N.; Savateev, A.; Ribeiro, C.; Kühne, T. D.; Antonietti, M.; Teixeira, I. F. Sustainable oxidation catalysis supported by light: Fe-poly (heptazine imide) as a heterogeneous single-atom photocatalyst. *Appl. Catal., B* **2022**, *304*, No. 120965.
(30) Paul, S.; Kao, Y.; Ni, L.; Ehnert, R.; Herrmann-Geppert, I.; Krol, R.; Stark, R. W.; Jaegermann, W.; Kramm, U. I.; Bogdanoff, P. Influence of the Metal Center in M−N−C Catalysts on the CO_2 Reduction Reaction on Gas Diffusion Electrodes. *ACS Catal.* **2021**, *11*, 5850−5864.
(31) Liu, M.; Guo, L.; Jin, S.; Tan, B. Covalent triazine frameworks: synthesis and applications. *J. Mater. Chem. A* **2019**, *7*, 5153−5172.
(32) Geng, K.; He, T.; Liu, R.; Dalapati, S.; Tan, K. T.; Li, Z.; Tao, S.; Gong, Y.; Jiang, Q.; Jiang, D. *Chem. Rev.* **2020**, *120*, 8814−8933.
(33) Qian, Z.; Wang, Z. J.; Zhang, K. A. I. Covalent Triazine Frameworks as Emerging Heterogeneous Photocatalysts. *Chem. Mater.* **2021**, *33*, 1909−1926.
(34) Raja, S.; Hamouda, A. E. I.; de Toledo, M. A. S.; Hu, C.; Bernardo, M. P.; Schalla, C.; Leite, L. S. F.; Buhl, E. M.; Dreschers, S.; Pich, A.; Zenke, M.; Mattoso, L. H. C.; Sechi, A. Functionalized Cellulose Nanocrystals for Cellular Labeling and Bioimaging. *Biomacromolecules* **2021**, *22*, 454−466.
(35) Inês, M.; Raja, S.; Tiago, S.; Suzete, A.; Érica Torres, T.; Ermelinda, M.; Baleizao, C. Two-photon absorption of perylene-3,4,9,10-tetracarboxylic acid diimides: effect of substituents in the bay. *Dyes Pigm.* **2021**, *193*, No. 109470.
(36) Li, Y.; Zhang, X.; Liu, D. Recent developments of perylene diimide (PDI) supramolecular photocatalysts: A review. *J. Photochem. Photobiol., C* **2021**, *48*, No. 100436.
(37) Zhao, N.; Liu, J.; Yang, F.; Lv, S.; Wang, J.; Wang, S. Easy Green Construction of a Universal Sensing Platform Based on Crystalline Polyimide Covalent Organic Frameworks with Sensitive Fluorescence Response to Metal Ions and Antibiotics. *ACS Appl. Bio Mater.* **2021**, *4*, 995−1002.
(38) Kim, H. M.; Jang, H. K.; Hwang, T. G.; Namgoong, J. W.; Kim, J. Y.; Yuk, S. B.; Lee, J. M.; Kim, J. P. Comparative study of the synthetic methods for perylene-based covalent triazine polyimides. *Dyes Pigm.* **2021**, *186*, No. 108968.
(39) Perfecto-Irigaray, M.; Merino-Garcia, I.; Albo, J.; Beobide, G.; Castillo, O.; Luque, A.; Pérez-Yáñez, S. Copper(II)-porphyrin functionalized titanium(IV) metal-organic aerogels for the visible-light driven conversion of CO_2 to alcohols. *Mater. Today Energy* **2023**, *36*, No. 101346.
(40) Landaluce, N.; Perfecto-Irigaray, M.; Albo, J.; Beobide, G.; Castillo, O.; Irabien, A.; Luque, A.; Méndez, A. S. J.; Platero-Prats, A. E.; Pérez-Yáñez, S. Copper(II) invigorated EHU-30 for continuous electroreduction of CO_2 into value-added chemicals. *Sci. Rep.* **2022**, *12*, No. 8505.
(41) Angulo-Ibáñez, A.; Perfecto-Irigaray, M.; Merino-Garcia, I.; Luengo, N.; Goitandia, A. M.; Albo, J.; Aranzabe, E.; Beobide, G.; Castillo, O.; Pérez-Yáñez, S. Metal-organic aerogels based on titanium(IV) for visible-light conducted CO_2 photoreduction to alcohols. *Mater. Today Energy* **2022**, *30*, No. 101178.
(42) Albo, J.; Perfecto-Irigaray, M.; Beobide, G.; Irabien, A. Cu/Bi metal-organic framework-based systems for an enhanced electrochemical transformation of CO_2 to alcohols. *J. CO_2 Util.* **2019**, *33*, 157−165.
(43) Santos-Lorenzo, J.; José-Veladoa, R. S.; Albob, J.; Beobidea, G.; Castañoc, P.; Castilloa, O.; Luquea, A.; Pérez-Yáñez, S. A straightforward route to obtain zirconium based metal-organic gels. *Microporous Mesoporous Mater.* **2019**, *284*, 128−132.
(44) Perfecto-Irigaray, M.; Albo, J.; Beobide, G.; Castillo, O.; Irabienb, A.; Perez-Yáñez, S. Synthesis of heterometallic metal−organic frameworks and their performance as electrocatalyst for CO_2 reduction. *RSC Adv.* **2018**, *8*, 21092−21099.
(45) Albo, J.; Vallejo, D.; Beobide, G.; Castillo, O.; Castaño, P.; Irabien, A. Copper-Based Metal−Organic Porous Materials for CO_2 Electrocatalytic Reduction to Alcohols. *ChemSusChem* **2017**, *10*, 1100−1109.
(46) Zhou, J.; Wang, Y.; Cui, Z.; Hu, Y.; Hao, X.; Wang, Y.; Zou, Z. Ultrathin conjugated polymer nanosheets as highly efficient photocatalyst for visible light driven oxygen activation. *Appl. Catal., B* **2020**, *277*, No. 119228.
(47) Wan, C.; Yi, J.; Cao, R.; Huang, Y. Conductive Metal/Covalent Organic Fmeworks for CO_2 Electro-reduction. *Chin. J. Struct. Chem.* **2022**, *41*, 2205001−2205014.
(48) Li, X.; Chen, Y.; Zhan, X.; Xu, Y.; Hao, L.; Xu, L.; Li, X.; Umer, M.; Tan, X.; Han, B.; Robertson, A. W.; Sun, Z. Strategies for enhancing electrochemical CO_2 reduction to multi-carbon fuels on copper. *Innovation Mater.* **2023**, *1*, No. 100014.
(49) Jiang, X.; Li, X.; Kong, Y.; Deng, C.; Li, X.; Hu, Q.; Yang, H.; He, C. A hierarchically structured tin-cobalt composite with an enhanced electronic effect for high-performance CO_2 electroreduction in a wide potential range. *J. Energy Chem.* **2023**, *76*, 462−469.
(50) Yang, H.; Lin, Q.; Zhang, C.; Yu, X.; Cheng, Z.; Li, G.; Hu, Q.; Ren, X.; Zhang, Q.; Liu, J.; He, C. Carbon dioxide electroreduction on

https://doi.org/10.1021/acs.energyfuels.3c03268
Energy Fuels XXXX, XXX, XXX−XXX

single-atom nickel decorated carbon membranes with industry compatible current densities. *Nat. Commun.* **2020**, *11*, No. 593.
(51) Xie, L.; Yu, X.; Wang, S.; Wei, S.; Hu, Q.; Chai, X.; Ren, X.; Yang, H.; He, C. A Multiscale Strategy to Construct Cobalt Nanoparticles Confined within Hierarchical Carbon Nanofibers for Efficient CO_2 Electroreduction. *Small* **2022**, *18*, No. 2104958.
(52) Su, P.; Iwase, K.; Harada, T.; Kamiya, K.; Nakanishi, S. Covalent triazine framework modified with coordinatively-unsaturated Co or Ni atoms for CO_2 electrochemical reduction. *Chem. Sci.* **2018**, *9*, 3941−3947.
(53) Lu, C.; Yang, J.; Wei, S.; Bi, S.; Xia, Y.; Chen, M.; Hou, Y.; Qiu, M.; Yuan, C.; Su, Y.; Zhang, F.; Liang, H.; Zhuang, X. Atomic Ni Anchored Covalent Triazine Framework as High Efficient Electrocatalyst for Carbon Dioxide Conversion. *Adv. Funct. Mater.* **2019**, *29*, No. 1806884.
(54) Ma, L.; Hu, W.; Mei, B.; Liu, H.; Yuan, B.; Zang, J.; Chen, T.; Zou, L.; Zou, Z.; Yang, B.; Yu, Y.; Ma, J.; Jiang, Z.; Wen, K.; Yang, H. Covalent Triazine Framework Confined Copper Catalysts for Selective Electrochemical CO_2 Reduction: Operando Diagnosis of Active Sites. *ACS Catal.* **2020**, *10*, 4534−4542.
(55) Creissen, C. E.; Fontecave, M. Keeping sight of copper in single-atom catalysts for electrochemical carbon dioxide reduction. *Nat. Commun.* **2022**, *13*, No. 2280.
(56) Jiao, Y.; Zheng, Y.; Chen, P.; Jaroniec, M.; Qiao, S. Z. Molecular scaffolding strategy with synergistic active centers to facilitate electrocatalytic CO_2 reduction to hydrocarbon/alcohol. *J. Am. Chem. Soc.* **2017**, *139*, 18093−18100.
(57) Raciti, D.; Wang, Y.; Park, J. H.; Wang, C. Three-Dimensional Hierarchical Copper-Based Nanostructures as Advanced Electrocatalysts for CO_2 Reduction. *ACS Appl. Energy Mater.* **2018**, *1*, 2392−2398.
(58) Long, C.; Li, X.; Guo, J.; Shi, Y.; Liu, S.; Tang, Z. Electrochemical Reduction of CO_2 over Heterogeneous Catalysts in Aqueous Solution: Recent Progress and Perspectives. *Small Methods* **2018**, *3*, No. 1800369.
(59) Cometto, C.; Ugolotti, A.; Grazietti1, E.; Moretto, A.; Bottaro, G.; Armelao, L.; Valentin, C. D.; Calvillo, L.; Granozzi, G. Copper single-atoms embedded in 2D graphitic carbon nitride for the CO_2 reduction. *npj 2D Mater. Appl.* **2021**, *5*, No. 63.
(60) Cai, Y.; Fu, J.; Zhou, Y.; Chang, Y.; Min, Q.; Zhu, J.; Lin, Y.; Zhu, W. Insights on forming N, O-coordinated Cu single atom catalysts for electrochemical reduction CO_2 to methane. *Nat. Commun.* **2021**, *12*, No. 586.
(61) Xu, H.; Rebollar, D.; He, H.; Chong, L.; Liu, Y.; Liu, C.; Sun, C.; Li, T.; Muntean, J. V.; Winans, R. E.; Liu, D.; Xu, T. Highly selective electrocatalytic CO_2 reduction to ethanol by metallic clusters dynamically formed from atomically dispersed copper. *Nat. Energy* **2020**, *5*, 623−632.
(62) Ma, W.; He, X.; Wang, W.; Xie, S.; Zhang, Q.; Wang, Y. Electrocatalytic reduction of CO_2 and CO to multi-carbon compounds over Cu-based catalysts. *Chem. Soc. Rev.* **2021**, *50*, 12897−12914.
(63) Qu, Y.; Li, Z.; Chen, W.; Lin, Y.; Yuan, T.; Yang, Z.; Zhao, C.; Wang, J.; Zhao, C.; Wang, X.; Zhou, F.; Zhuang, Z.; Wu, Y.; Li, Y. Direct transformation of bulk copper into copper single sites via emitting and trapping of atoms. *Nat. Catal* **2018**, *1*, 781−786.
(64) Wei, S.; Jiang, X.; He, C.; Wang, S.; Hu, Q.; Chai, X.; Ren, X.; Yang, H.; He, C. Construction of single-atom copper sites with low coordination number for efficient CO_2 electroreduction to CH_4. *J. Mater. Chem. A* **2022**, *10*, 6187−6192.
(65) Oliveira, J. A.; Silva, R. R. M.; da Silva, G. T. S. T.; Torres, J. A.; Vali, A.; Ribeiro, C.; Rajeshwar, K.; Ruotolo, L. A. M. Copper vanadates: Targeted synthesis of two pure phases and use in a photoanode/cathode setup for selective photoelectrochemical conversion of carbon dioxide to liquid fuel. *Mater. Res. Bull.* **2022**, *149*, No. 111716.
(66) Pieta, I. S.; Kadam, R. G.; Pieta, P.; Mrdenovic, D.; Nowakowski, R.; Bakandritsos, A.; Tomanec, O.; Petr, M.; Otyepka, M.; Kostecki, R.; Khan, M. A. M.; Zboril, R.; Gawande, M. B. The Hallmarks of Copper Single Atom Catalysts in Direct Alcohol Fuel Cells and Electrochemical CO_2 Fixation. *Adv. Mater. Interfaces* **2021**, *8*, No. 2001822.
(67) Yang, Z.; Chen, B.; Chen, W.; Qu, Y.; Zhou, F.; Zhao, C.; Xu, Q.; Zhang, Q.; Duan, X.; Wu, Y. Directly transforming copper (I) oxide bulk into isolated single-atom copper sites catalyst through gas-transport approach. *Nat. Commun.* **2019**, *10*, No. 3734.
(68) Wu, H. H.; Li, H. B.; Zhao, X. F.; Liu, Q. F.; Wang, J.; Xiao, J. P.; Xie, S. H.; Si, R.; Yang, F.; Miao, S.; Guo, X. G.; Wang, G. X.; Bao, X. H. Highly doped and exposed Cu(I)-N active sites within graphene towards efficient oxygen reduction for zinc-air batteries. *Energy Environ. Sci.* **2016**, *9*, 3736−3745.
(69) Gu, Z. X.; Yang, N.; Han, P.; Kuang, M.; Mei, B. B.; Jiang, Z.; Zhong, J.; Li, L.; Zheng, G. F. Oxygen vacancytuning toward efficient electrocatalytic CO_2 reduction to C_2H_4. *Small Methods* **2019**, *3*, No. 1800449.
(70) Zou, J.; Lee, C.; Wallace, G. G. Boosting Formate Production from CO_2 at High Current Densities Over a Wide Electrochemical Potential Window on a SnS Catalyst. *Adv. Sci.* **2021**, *8*, No. 2004521.
(71) Gawande, M. B.; Goswami, A.; Felpin, F.; Asefa, T.; Huang, X.; Silva, R.; Zou, X.; Zboril, R.; Varma, R. S. Cu and Cu-Based Nanoparticles: Synthesis and Applications in Catalysis. *Chem. Rev.* **2016**, *116*, 3722−3811.
(72) Zhao, J.; Xue, S.; Barber, J.; Zhou, Y.; Meng, J.; Ke, X. An overview of Cu-based heterogeneous electrocatalysts for CO_2 reduction. *J. Mater. Chem. A* **2020**, *8*, 4700−4734.
(73) Nitopi, S.; Bertheussen, E.; Scott, S. B.; Liu, X.; Engstfeld, A. K.; Horch, S.; Seger, B.; Stephens, I. E. L.; Chan, K.; Hahn, C.; Nørskov, J. K.; Jaramillo, T. F.; Chorkendorff, I. Progress and Perspectives of Electrochemical CO_2 Reduction on Copper in Aqueous Electrolyte. *Chem. Rev.* **2019**, *119*, 7610−7672.

https://doi.org/10.1021/acs.energyfuels.3c03268
Energy Fuels XXXX, XXX, XXX−XXX